Channel Modeling and Signal Transmission for Land Mobile Satellite MIMO

Hongwei Peng*, Chenhao Qi*, Yang Chen*, Qian Zhang†, Dong Chen† and Rui Ding†
*School of Information and Science and Engineering, Southeast University, Nanjing, China
†Institute of Telecommunication Satellite, China Academy of Space Technology, Beijing, China
Email: {hwpeng, qch,cheny}@seu.edu.cn

GLOBECOM 2021 - 2021 IEEE Global Communications Conference | 978-1-7281-8104-2/21/$31.00 ©2021 IEEE | DOI: 10.1109/GLOBECOM46510.2021.9685823

***Abstract*—In this paper, a land mobile satellite (LMS) multiple-input multiple-output (MIMO) is considered, where two satellites simultaneously communicate with a mobile user terminal (UT). Spatial degree of freedom brought by the two satellites is introduced in the channel modeling, aside of other channel parameters including time correlation, shadowing, multipath fading and Doppler effect. Then an algorithm table using Markov multiple-state transition is provided to generate the LMS MIMO channels. Based on the modeled LMS MIMO channels, signal transmission between two satellites and the UT using space-time block coding is considered. Simulation results show that compared to the single satellite communications, the dual-satellite MIMO communications can achieve better bit error rate performance under the same signal-to-noise-ratio condition. In particular, the performance of dual-satellite single-polarization communications is slightly worse than that of single-satellite dual-polarization communications, since the spatial correlation is stronger than the polarization correlation.**

***Index Terms*—Channel modeling, land mobile satellite (LMS), multiple-input multiple-output (MIMO), signal transmission, space-time block coding**

I. Introduction

The land mobile satellite (LMS) communication system will play an important role in future wireless systems owing to its advantages such as convenient deployment and being immune to influences of the geographical environment [1], [2]. The successful application of multiple-input multiple-output (MIMO) technology in terrestrial wireless communications has promoted its extension in satellite communications [3], [4]. But due to the limitation of size, weight and power consumption of the satellite, the LMS MIMO is different from the terrestrial MIMO [5]. Currently, the LMS MIMO is mainly constructed by dual polarization on a single satellite [6]. A state model based on semi-Markov chains assuming a log-normal state duration distribution is proposed to model the LMS MIMO channels [7]. On the other hand, the characteristics of signal propagation from the satellite to mobile user terminals (UTs) are analyzed in detail but without consideration of different channel states [8]. By combining the work in [7] and [8], the channel factors during signal propagation from the satellite to mobile UT are comprehensively analyzed [9]. In particular, an algorithm is also presented in [9] to model dual-polarized LMS MIMO channel, which investigates almost all channel factors including temporal and polarization correlation, line-of-sight (LOS) shadowing, multipath effect, cross-polar discrimination of antennas, cross-polar coupling of environments, elevation angle, user environments and Doppler frequency shift.

In this paper, we further consider the LMS MIMO with two geosynchronous earth orbit (GEO) satellites, which simultaneously communicate with a mobile UT. Spatial degree of freedom brought by the two satellites is introduced in the channel modeling, aside of other channel parameters including time correlation, shadowing, multipath fading and Doppler effect. Then an algorithm table using Markov multiple-state transition is provided to generate the LMS MIMO channels. Based on the modeled LMS MIMO channels, signal transmission between two satellites and the UT using space-time block coding is considered.

The notations used in this paper are summarized as follows. Symbols for matrices and vectors are in boldface. The symbols a, $\boldsymbol{a}$ and $\boldsymbol{A}$ denote a scalar, a vector and a matrix, respectively. The symbols $[\cdot]_{m,n}$, $(\cdot)^T$, $(\cdot)^H$, $\otimes$, $\boldsymbol{I}_L$, $\mathcal{U}$, $\mathcal{N}$ and $\mathcal{CN}$ denote the entry on the mth row and nth column of a matrix, the matrix transpose, the matrix conjugate transpose (Hermitian), Kronecker product operator, the identity matrix of size L, the uniformly distribution, the Gaussian distribution and the complex Gaussian distribution, respectively. The operator round(x) rounds x to the nearest integer. The operator vec$(\boldsymbol{A})$ denotes the vectorization of the matrix $\boldsymbol{A}$.

II. System model of DSSP LMS MIMO

The block diagram of the dual-satellite single-polarization (DSSP) LMS MIMO system is shown in the Fig. 1. Each satellite is equipped with a single-polarization antenna using the left-hand circular polarization (LHCP), while the UT is equipped with two antennas with the same polarization mode. The LMS MIMO downlink channel can be expressed by 2×2 channel matrix as

$$\boldsymbol{H} \triangleq \begin{bmatrix} h_{11} & h_{12} \\ h_{21} & h_{22} \end{bmatrix} \tag{1}$$

where h_{mn} is the complex-valued channel gain between the nth satellite and the mth receiving antenna of the UT, for $m, n \in \{1, 2\}$. The envelope of h_{mn}, denoted as $|h_{mn}|$, obeys the Loo distribution, since it has already been extensively used and validated by the DVB-SH standards. According to

978-1-7281-8104-2/21/$31.00 ©2021 IEEE

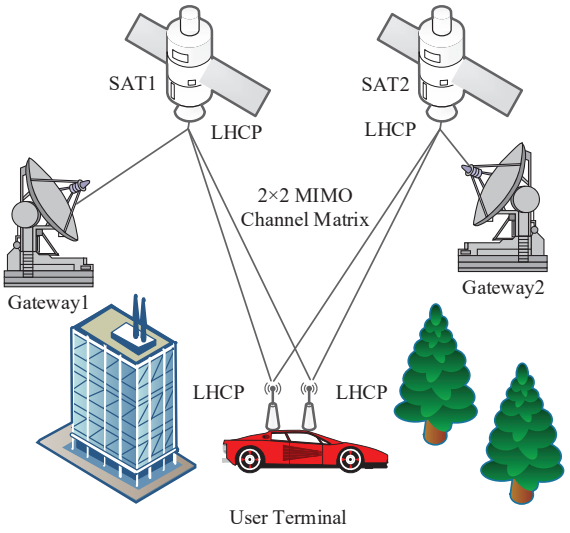

Fig. 1. Block diagram of dual-satellite single-polarization LMS MIMO.

the Loo distribution, we have

$$\boldsymbol{H} = \overline{\boldsymbol{H}} + \widetilde{\boldsymbol{H}} \tag{2}$$

where

$$\overline{\boldsymbol{H}} \triangleq \begin{bmatrix} \overline{h}_{11} & \overline{h}_{12} \\ \overline{h}_{21} & \overline{h}_{22} \end{bmatrix} \text{ and } \widetilde{\boldsymbol{H}} \triangleq \begin{bmatrix} \widetilde{h}_{11} & \widetilde{h}_{12} \\ \widetilde{h}_{21} & \widetilde{h}_{22} \end{bmatrix} \tag{3}$$

represent the large-scale LOS shadowing component and small-scale multipath fading component, respectively. We further denote

$$\overline{h}_{mn} = \left|\overline{h}_{mn}\right| e^{j\overline{\phi}_{mn}} \tag{4}$$

and

$$\widetilde{h}_{mn} = \left|\widetilde{h}_{mn}\right| e^{j\widetilde{\phi}_{mn}} \tag{5}$$

where $\left|\overline{h}_{mn}\right|$ and $\overline{\phi}_{mn}$ are the envelope and phase of $\overline{h}_{mn}$, respectively, and $\left|\widetilde{h}_{mn}\right|$ and $\widetilde{\phi}_{mn}$ are the envelope and phase of $\widetilde{h}_{mn}$, respectively. $\left|\overline{h}_{mn}\right|$ and $\left|\widetilde{h}_{mn}\right|$ obey the log-normal distribution and the Rayleigh distribution, respectively. Both $\overline{\phi}_{mn}$ and $\widetilde{\phi}_{mn}$ are independently and uniformly distributed over $[0, 2\pi)$.

To simplify the notations, we denote $r \triangleq |h_{mn}|$. Then the probability density function of r can be expressed as

$$p(r) = \frac{r}{b_0\sqrt{2\pi d_0}} \int_0^\infty \frac{1}{z} e^{-\frac{(\ln z-\mu)^2}{2d_0} - \frac{r^2+z^2}{2b_0}} I_0\left(\frac{rz}{b_0}\right) \mathrm{d}z \tag{6}$$

where $I_0(\cdot)$ is the zeroth order modified Bessel function, and the variables μ, d_0 and b_0 are related to α, ψ and MP, respectively, with the following relations

$$\alpha = 20\log_{10}(e^{\mu}), \tag{7}$$

$$\psi = 20\log_{10}(e^{\sqrt{d_0}}) \tag{8}$$

and

$$MP = 20\log_{10}(2b_0). \tag{9}$$

In fact, α, ψ and MP are the mean, standard deviation of $\overline{h}_{mn}$ and the average power of $\widetilde{h}_{mn}$, all in the unit of dB. Experimental datasets of α, ψ and MP are provide in [10].

III. Analysis of Several Effects on DSSP LMS MIMO

A. Markov state transition

The movement of UT with a certain speed v makes the LMS channel coherent in time. The time-varying property of the LMS channel is modeled by a four-state Markov transition process with given state transition probability matrix

$$\boldsymbol{P} \triangleq \begin{bmatrix} p_{11} & p_{12} & p_{13} & p_{14} \\ p_{21} & p_{22} & p_{23} & p_{24} \\ p_{31} & p_{32} & p_{33} & p_{34} \\ p_{41} & p_{42} & p_{43} & p_{44} \end{bmatrix} \tag{10}$$

and state probability vector $\boldsymbol{w}$ [10]. We denote the four states by S_1, S_2, S_3 and S_4, where p_{mn} denotes the transition probability from S_m to S_n, for $m, n \in \{1, 2, 3, 4\}$. Note that the summation of four entries in each row or each column equals one. From each satellite to the UT, there are two channels, either both channels in a good state or both channels in a bad state, which results in totally four combinations for two satellites, i.e., {bad, bad}, {bad, good}, {good,bad} and {good, good}. The minimum duration of each state is L_f/v, where L_f is the state-related distance and usually set to be $3-8$m [11]. It is assumed that α, ψ and MP keep constant within each state [9].

B. Temporal correlation

The samples of the small-scale multipath fading component are randomly generated when the UT moves in a distance L_m. Note that L_m is usually set as λ/F, where λ is the signal wavelength and F is a factor between 8 and 10 [9].

The samples of the large-scale LOS shadowing component are randomly generated when the UT moves in a distance L_d. Note that L_d is usually set to be $1-3$m. In fact, the temporal correlation of large-scale LOS shadowing component can be introduced by a low-pass infinite impulse response (IIR) filter [12]. The specific process is listed as follows.

First, M samples, denoted as $\{x_m, m = 1, 2, \cdots, M\}$, are independently generated obeying the Gaussian distribution with zero mean and unit variance, where $M \triangleq \text{round}(L_f/L_m)$. Then these samples pass through a low-pass IIR filter to introduce the temporal correlation. The relation of the input x_n and the output y_n of the IIR filter can be described as

$$y_n = x_n + A \cdot y_{n-1} \tag{11}$$

where $A \triangleq e^{-vT/L_d}$ and the sampling time $T \triangleq \lambda/(Fv)$. To ensure that the sample variance remains unchanged after filtering, $\{y_m, m = 1, 2, \cdots, M\}$ needs to be multiplied by $\sqrt{1-A^2}$ in amplitude.

C. Doppler effect

Due to the movement of the UT, the actual received signal spectrum will be affected by the Doppler effect. A low-pass Butterworth filter is used to introduce Doppler frequency shift to the small-scale multipath fading component [11]. The magnitude square function of the Butterworth filter is expressed as

$$|H_{\text{buff}}(f)|^2 = \frac{B}{1+(f/f_c)^{2k}} \tag{12}$$

where f_c is the cutoff frequency, and k is the order of the filter. Since the signal variance will change before and after filtering, the multiplicative factor B is introduced for adjustment. It is assumed that for every L_d of UT movement, the phase of the large-scale LOS shadowing component increases linearly with a fixed value

$$\triangle\phi = 2\pi\frac{\cos\theta}{F} \tag{13}$$

where θ is the elevation angle of the satellite at UT.

D. Spatial correlation

Now we introduce spatial correlation among the LMS channels.

1) Spatial correlation of large-scale LOS shadowing component: Given a 2×2 channel matrix $\overline{\boldsymbol{H}}_w$ whose entry independently obeys Gaussian distribution with zero mean and unit variance, we introduce the spatial correlation to $\overline{\boldsymbol{H}}_w$ by

$$\text{vec}(\overline{\boldsymbol{H}}_s) = \overline{\boldsymbol{C}}_s^{1/2}\text{vec}(\overline{\boldsymbol{H}}_w) \tag{14}$$

where $\overline{\boldsymbol{C}}_s$ is defined to be a 4×4 positive semidefinite Hermitian matrix as

$$\overline{\boldsymbol{C}}_s = \begin{bmatrix} 1 & 1 & \overline{\rho}_{LN} & \overline{\rho}_{LN} \\ 1 & 1 & \overline{\rho}_{LN} & \overline{\rho}_{LN} \\ \overline{\rho}_{LN} & \overline{\rho}_{LN} & 1 & 1 \\ \overline{\rho}_{LN} & \overline{\rho}_{LN} & 1 & 1 \end{bmatrix}. \tag{15}$$

The measurement data of $\overline{\rho}_{LN}$ in certain environment is given in [13]–[15]. Then the large-scale LOS shadowing component with spatial correlation can be generated by

$$\text{vec}(\overline{\boldsymbol{H}}_{LN}) = 10^{\text{vec}(\overline{\boldsymbol{H}}_s)\frac{\psi}{20}+\frac{\alpha}{20}}. \tag{16}$$

2) Spatial correlation of small-scale multipath fading component: Given a 2×2 channel matrix $\widetilde{\boldsymbol{H}}_w$ whose entry independently obeys complex Gaussian distribution with zero mean and unit variance, we introduce the spatial correlation to $\widetilde{\boldsymbol{H}}_w$ by

$$\text{vec}(\widetilde{\boldsymbol{H}}_s) = \widetilde{\boldsymbol{C}}_s^{1/2}\text{vec}(\widetilde{\boldsymbol{H}}_w) \tag{17}$$

where $\widetilde{\boldsymbol{C}}_s$ is defined to a 4×4 positive semidefinite Hermitian matrix. We have

$$\widetilde{\boldsymbol{C}}_s = \widetilde{\boldsymbol{R}}_t^T \otimes \widetilde{\boldsymbol{R}}_r \tag{18}$$

where $\widetilde{\boldsymbol{R}}_r$ and $\widetilde{\boldsymbol{R}}_t$ are 2×2 order positive semidefinite Hermitian covariance matrices of the small-scale multipath fading component at the receiving end and the transmitting side, respectively. We can derive them as

$$\widetilde{\boldsymbol{R}}_r = E\{\widetilde{\boldsymbol{H}}_s\widetilde{\boldsymbol{H}}_s^H\} = \begin{bmatrix} 1 & \widetilde{\rho}_r \\ \widetilde{\rho}_r & 1 \end{bmatrix} \tag{19}$$

and

$$\widetilde{\boldsymbol{R}}_t = E\{\widetilde{\boldsymbol{H}}_s^H\widetilde{\boldsymbol{H}}_s\} = \begin{bmatrix} 1 & \widetilde{\rho}_t \\ \widetilde{\rho}_t & 1 \end{bmatrix}. \tag{20}$$

They are affected by the local environment of the UT, the elevation angle of the satellite, the distance between the two receiving antenna, and etc.

Algorithm 1 Channel Modeling Algorithm

Input: $\boldsymbol{P}, S_b, L, M$.
Initialization: Set $\boldsymbol{H}_i,\ i=1,2,\ldots,LM$ all zero.
for $l=1,\cdots,L$ **do**
  Generate a random variable $u\sim\mathcal{U}[0,1]$.
  for $m=1,2,3,4$ **do**
    if $u\le\sum_{n=1}^{m}p_{bn}$ **then**
      $S_b\leftarrow S_m$. Break.
    else
      $m=m+1$.
    end if
  end for
  Obtain α,ψ and MP for S_b.
  Generate initial phase $\phi_0\sim\mathcal{U}(0,2\pi)$.
  Generate $\boldsymbol{g}_{mn}^w\sim\mathcal{N}(0,\boldsymbol{I}_M), m,n\in\{1,2\}$.
  Input $\boldsymbol{g}_{mn}^w$ to the IIR filter in (12), and then multiply the filter output with $\sqrt{1-A^2}$, resulting in $\boldsymbol{g}_{mn}^t, m,n\in\{1,2\}$.
  for $k=1,\cdots,M$ **do**
    $\boldsymbol{G}^t(m,n)=\boldsymbol{g}_{mn}^t(k), m,n\in\{1,2\}$.
    Obtain $\text{vec}(\boldsymbol{G}^s)$ based on $\boldsymbol{G}^t$ according to (14).
    Obtain $\text{vec}(\boldsymbol{G}^{LN})$ based on $\boldsymbol{G}^s$ according to (16).
    $\text{vec}(\boldsymbol{G})=\text{vec}(\boldsymbol{G}^{LN})e^{j(\phi_0+k\triangle\phi)}$ according to (13).
    $\boldsymbol{H}_{(l-1)M+k}=\boldsymbol{G}$.
  end for
  Generate $\boldsymbol{q}_{mn}^w\sim\mathcal{CN}(0,\boldsymbol{I}_M), m,n\in\{1,2\}$.
  Input $\boldsymbol{q}_{mn}^w$ to the Butterworth filter in (12), and then multiply the filter output with $B\sqrt{b_0}$, resulting in $\boldsymbol{q}_{mn}^t, m,n\in\{1,2\}$.
  for $k=1,\cdots,M$ **do**
    $\boldsymbol{Q}^t(m,n)=\boldsymbol{q}_{mn}^t(k), m,n\in\{1,2\}$.
    Obtain $\text{vec}(\boldsymbol{Q})$ based on $\boldsymbol{Q}^t$ according to (17).
    $\boldsymbol{H}_{(l-1)M+k}=\boldsymbol{Q}+\boldsymbol{H}_{(l-1)M+k}$.
  end for
end for
Output: $\boldsymbol{H}_i,\ i=1,2,\ldots,LM$.

IV. Algorithm for modeling DSSP LMS MIMO channels

Considering several factors that affect channel modeling in Section III, in this section we will propose Algorithm 1 to model the DSSP LMS MIMO channels.

As shown in the algorithm table, first we input the state transition matrix $\boldsymbol{P}$, the current channel state S_b, the number of inner-loop iterations M, and the number of outer-loop iterations $L = \text{round}(L_u/L_f)$, where L_u is the moving distance of the UT. Therefore, we have totally LM samples, where in each sample we generate a 2×2 channel matrix expressed in (1). The final output of the algorithm table is a serial of channel matrix $\{\boldsymbol{H}_i,\ i = 1, 2, \ldots, LM\}$, which is initialized to be zero.

At the beginning of each outer-loop iteration, a uniformly distributed random variable $u \sim \mathcal{U}[0, 1]$ is generated to describe the transition process of different channel states including S_1, S_2, S_3, and S_4. Once the channel state is given, the Loo model parameters α, ψ and MP are determined according to [10]. These steps are summarized from step 4 to step 12.

From step 13 to step 22, the large-scale LOS shadowing component of the DSSP LMS MIMO channels is generated. Then four vectors $\boldsymbol{g}_{mn}^w, m, n \in \{1, 2\}$ are generated, where the entries of each vector obey the cyclically symmetric Gaussian distribution with zero mean and unit variance. We introduce the temporal correlation to each of $\boldsymbol{g}_{mn}^w, m, n \in \{1, 2\}$ by passing it through the low-pass IIR filter described by (11), and then multiply the amplitude of the filter output by $\sqrt{1 - A^2}$ to ensure that the variance before and after filtering remains unchanged. During the first inner-loop iterations from step 16 to step 22, we consider the spatial correlation and Doppler effect according to (III-D) and (III-C), respectively. In particular, we introduce the spatial correlation by step 18 and step 19, while we consider the Doppler effect in step 20.

From step 23 to step 30, the small-scale multipath fading component of the DSSP LMS MIMO channels is generated. Then four vectors $\boldsymbol{q}_{mn}^w$ are generated, where the entries of each vector obey the cyclically symmetric complex Gaussian distribution with zero mean and unit variance. We introduce the Doppler effect to each of $\boldsymbol{q}_{mn}^w, m, n \in \{1, 2\}$ by passing it through the Butterworth filter described by (12), and then multiply it by B to ensure that the variance before and after filtering remains unchanged. We further multiply it by $\sqrt{b_0}$ to introduce the multipath fading, where $\sqrt{b_0}$ is given in (9). During the second inner-loop iterations from step 25 to step 29, we introduce the spatial correlation to the small-scale multipath fading component according to (17).

In step 21, we store the generated large-scale LOS shadowing component to $\boldsymbol{H}_i, i = 1, 2, \ldots, LM$. In step 28, we combine the generated large-scale LOS shadowing component and small-scale multipath fading component. Finally, we output $\boldsymbol{H}_i, i = 1, 2, \ldots, LM$ as the generated DSSP LMS MIMO channels.

V. Signal Transmission Using Space-Time Block Coding

Space-time block coding, as a coding technique suitable for multiple antennas, can fully explore the diversity gain of MIMO system [16]. It combines the advantages of space diversity and time diversity, introduces the correlation between the space domain and the time domain between the signals sent by different antennas, and can provide a certain diversity gain and multiplexing gain. Therefore, space-time block coding can improve the effectiveness and reliability of wireless transmission without increasing the bandwidth or transmission power.

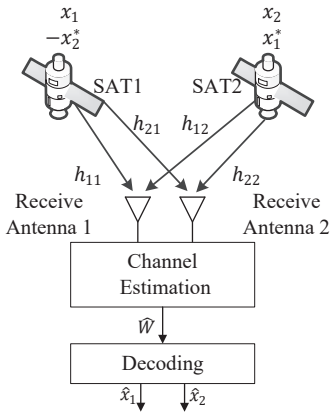

Fig. 2. Block diagram of DSSP LMS MIMO using space-time block coding.

As shown in Fig. 2, we give the block diagram of the popular Alamouti space-time block coding scheme. The channel coefficient from the nth transmitting antenna to the mth receiving antenna is denoted by $h_{mn}, m, n \in \{1, 2\}$, which can form a channel matrix $\boldsymbol{H}$ in (1). Suppose that $\boldsymbol{H}$ keeps constant during the channel coherence time, e.g., two consecutive symbol periods or time slots. Suppose the symbols transmitted by the two satellites in the first time slot are denoted as x_1 and x_2, respectively. According to the Alamouti scheme, in the second time slot, the two satellites transmit $-x_2^*$ and x_1^*, respectively. The signal received by the two antennas at UT is denoted as y_{11} and y_{12} for the first time slot, and y_{21} and y_{22} for the second time slot. Then we have

$$\begin{aligned} y_{11} &= h_{11}x_1 + h_{12}x_2 + \eta_{11}, \\ y_{12} &= h_{21}x_1 + h_{22}x_2 + \eta_{12}, \\ y_{21} &= -h_{11}x_2^* + h_{12}x_1^* + \eta_{21}, \\ y_{22} &= -h_{21}x_2^* + h_{22}x_1^* + \eta_{22}, \end{aligned} \tag{21}$$

where $\eta_{mn}, m, n \in \{1, 2\}$ represents the additive white Gaussian noise. Taking the conjugate for both sides of the last two equations in (21), we have

$$\begin{aligned} y_{21}^* &= -h_{11}^*x_2 + h_{12}^*x_1 + \eta_{21}^*, \\ y_{22}^* &= -h_{21}^*x_2 + h_{22}^*x_1 + \eta_{22}^*. \end{aligned} \tag{22}$$

In fact, we can rewrite in matrix form as

$$\boldsymbol{y} = \boldsymbol{W}\boldsymbol{x} + \boldsymbol{\eta} \tag{23}$$

where $\boldsymbol{y} \triangleq [y_{11}, y_{12}, y_{21}^*, y_{22}^*]^T$, $\boldsymbol{x} \triangleq [x_1, x_2]^T$, $\boldsymbol{\eta} \triangleq$

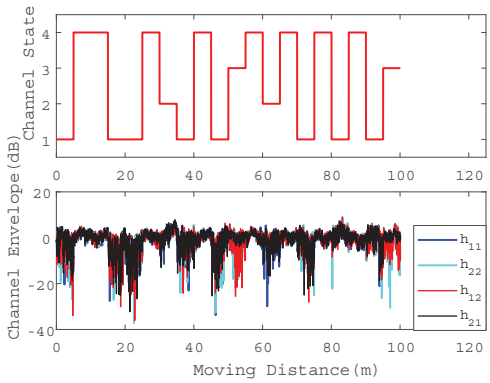

Fig. 3. Illustration of the channel state transition in the urban environment.

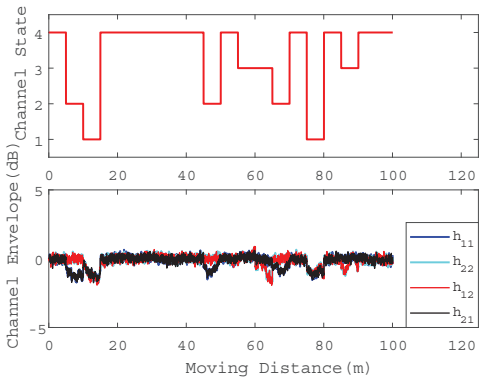

Fig. 4. Illustration of the channel state transition in the open environment.

$[\eta_{11}, \eta_{12}, \eta_{21}^*, \eta_{22}^*]^T$ and

$$\boldsymbol{W} \triangleq \begin{bmatrix} h_{11} & h_{12} \\ h_{21} & h_{22} \\ h_{12}^* & -h_{11}^* \\ h_{22}^* & -h_{21}^* \end{bmatrix}. \tag{24}$$

We denote the channel estimate of $\boldsymbol{W}$ as $\widehat{\boldsymbol{W}}$ for the UT. Then we multiply both sides of (23) by $\widehat{\boldsymbol{W}}^H$, resulting in

$$\widehat{\boldsymbol{W}}^H \boldsymbol{y} = (\widehat{\boldsymbol{W}}^H \boldsymbol{W})\boldsymbol{x} + \widehat{\boldsymbol{W}}^H \boldsymbol{\eta}. \tag{25}$$

Then an estimate of $\boldsymbol{x}$ can be expressed as

$$\widehat{\boldsymbol{x}} = (\widehat{\boldsymbol{W}}^H \boldsymbol{W})^{-1} \widehat{\boldsymbol{W}}^H \boldsymbol{y}. \tag{26}$$

If $\widehat{\boldsymbol{W}}$ is ideal, i.e., $\widehat{\boldsymbol{W}} = \boldsymbol{W}$, we have

$$\widehat{\boldsymbol{W}}^H \boldsymbol{W} = \left(|h_{11}|^2 + |h_{12}|^2 + |h_{21}|^2 + |h_{22}|^2 \right) \boldsymbol{I}_2 \triangleq d\boldsymbol{I}_2. \tag{27}$$

In this context, we have

$$\widehat{\boldsymbol{x}}_{\text{id}} = \frac{1}{d} \boldsymbol{W}^H \boldsymbol{y}. \tag{28}$$

After constellation demapping on $\widehat{\boldsymbol{x}}$, we can reconstruct the transmitted symbols by

$$\widehat{x}_1 = Q\big(\widehat{\boldsymbol{x}}(1)\big) \quad \text{and} \quad \widehat{x}_2 = Q\big(\widehat{\boldsymbol{x}}(2)\big) \tag{29}$$

where $Q(\cdot)$ represents the constellation demapping function.

VI. Simulation Results

The parameters for the simulation are set as follows. The working frequency of the LMS MIMO system is set to be 2.2 GHz at S band, which indicates the wavelength $\lambda = 0.1364$m. For the UT, the elevation angle θ is set to be 40° for both satellites but on the different side. The state-related distance L_f is set to be 5m. The speed of the moving UT is $v = 10$ m/s. The passband cutoff frequency of Butterworth filter described in (12) at 3dB and 100dB is set to be $0.9v/\lambda$ and $3v/\lambda$, respectively.

We first evaluate the channel modeling algorithm. As shown in Fig. 3, we illustrate the change of the channel state and channel envelop in urban environment. In Fig. 4, we illustrate the change of the channel state and channel envelop in open environment. It is seen from the figures that as the UT moves, the channel state transitions among four states S_1, S_2, S_3 and S_4. Since the urban environment is a richer scattering environment than the open environment, the channel gain of the former is smaller than that of the latter. Moreover, it is seen that the difference between $|h_{11}|$ and $|h_{21}|$ is smaller than that between $|h_{11}|$ and $|h_{12}|$. The reason is that $|h_{11}|$ and $|h_{21}|$ experience almost the same propagation environment, since the two antennas at the UT is relatively close to each other. But $|h_{11}|$ and $|h_{12}|$ are more different to each other, since the distance between two satellites is large and leads to different large-scale propagation. Similarly, the difference between $|h_{12}|$ and $|h_{22}|$ is smaller than that between $|h_{21}|$ and $|h_{22}|$.

We then compare the bit error rate (BER) performance for the DSSP, single-satellite dual-polarization (SSDP) and dual-satellite dual-polarization (DSDP) LMS MIMO. The performance of single-satellite single-polarization (SISO) is also provided for comparisons. It is seen that compared to the single satellite communications, the dual-satellite MIMO communications can achieve better BER performance under the same signal-to-noise-ratio (SNR) condition. The urban environment and the open environment are considered in Fig. 5 and Fig. 6, respectively. It is seen that the BER performance in open environment is better than that in urban environment, since the channel condition of the former is better than that of the latter. Since the satellite communications mainly rely on the LOS propagation, the rich scattering in the urban environment deteriorates the BER performance.

In both Fig. 5 and Fig. 6, the DSDP performs the best and the SISO is the worst. Under the same SNR condition, both the DSSP and SSDP outperform the SISO, but are worse than the DSDP. In particular, the SSDP is slightly better than the DSSP, since the polarization isolation is better than the spatial isolation, i.e., the spatial correlation is stronger than the polarization correlation. For the SISO, one single-polarization satellite and a UT with single antenna are considered in one time slot. For the DSSP, two single-polarization satellites

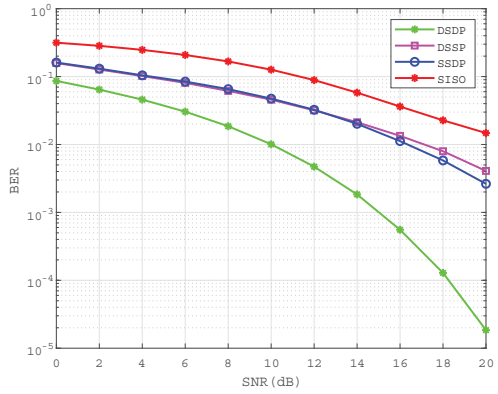

Fig. 5. BER comparisons in the urban environment.

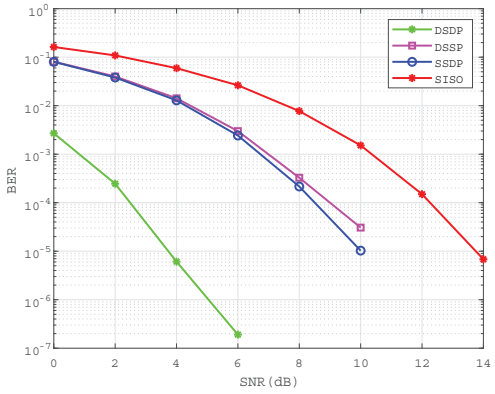

Fig. 6. BER comparisons in the open environment.

and a UT with two antennas are considered in two time slots, which leads $\boldsymbol{W}$ in (23) to be 4×2 in dimension. For the SSDP, a dual-polarization satellite and a UT with two antennas are considered in two time slots, which also leads $\boldsymbol{W}$ in (23) to be 4×2 in dimension. But for the DSDP, two dual-polarization satellites and a UT with four antennas are considered in four time slots, which leads $\boldsymbol{W}$ in (23) to be 16×4 in dimension. More rows than the columns of $\boldsymbol{W}$ indicates more measurements than the unknown variables, which can explain the best performance of the DSDP.

VII. Conclusions

In this paper, we have considered a LMS MIMO, where two satellites simultaneously communicate with a UT. Spatial degree of freedom brought by the two satellites has been introduced in the channel modeling, aside of other channel parameters including time correlation, shadowing, multipath fading and Doppler effect. Then an algorithm table using Markov multiple-state transition has been provided to generate the LMS MIMO channels. Based on the modeled LMS MIMO channels, signal transmission between two satellites and the UT using space-time block coding has been considered. Simulation results have shown that compared to the single satellite communications, the dual-satellite MIMO communications can achieve better BER performance under the same SNR condition. In particular, the performance of the DSSP is slightly worse than that of the SSDP, since the spatial correlation is stronger than the polarization correlation. Future work will be continued with the focus on the LMS MIMO signal processing.

Acknowledgment

This work is supported in part by the National Natural Science Foundation of China (NSFC) under Grant 62071116.

References

[1] Z. Lin, M. Lin, Y. Huang, T. d. Cola, and W.-P. Zhu, "Robust multi-objective beamforming for integrated satellite and high altitude platform network with imperfect channel state information," *IEEE Trans. Signal Process.*, vol. 67, no. 24, pp. 6384–6396, Nov. 2019.

[2] C. Qi and X. Wang, "Precoding design for energy efficiency of multibeam satellite communications," *IEEE Commun. Lett.*, vol. 22, no. 9, pp. 1826–1829, Sep. 2018.

[3] Z. Lin, C. Yin, J. Ouyang, X. Wu, and A. D. Panagopoulos, "Robust secrecy energy efficient beamforming in satellite communication systems," in *Proc. IEEE Int. Conf. Commun. (ICC)*, Shanghai, China, May 2019, pp. 1–5.

[4] H. Chen and C. Qi, "User grouping for sum-rate maximization in multiuser multibeam satellite communications," in *Proc. IEEE Int. Conf. Commun. (ICC)*, Shanghai, China, May 2019, pp. 1–6.

[5] C. Qi, H. Chen, Y. Deng, and A. Nallanathan, "Energy efficient multicast precoding for multiuser multibeam satellite communications," *IEEE Wirel. Commun. Lett.*, vol. 9, no. 4, pp. 567–570, Apr. 2020.

[6] P.-D. Arapoglou, K. Liolis, M. Bertinelli, A. Panagopoulos, P. Cottis, and R. De Gaudenzi, "MIMO over satellite: A review," *IEEE Commun. Surv. Tutor.*, vol. 13, no. 1, pp. 27–51, First Quarter 2011.

[7] P. Petropoulou, E. T. Michailidis, A. D. Panagopoulos, and A. G. Kanatas, "Radio propagation channel measurements for multi-antenna satellite communication systems: A survey," *IEEE Antennas Propag. Mag.*, vol. 56, no. 6, pp. 102–122, Dec. 2014.

[8] K. P. Liolis, J. Gomez-Vilardebo, E. Casini, and A. I. Perez-Neira, "Statistical modeling of dual-polarized MIMO land mobile satellite channels," *IEEE Trans. Commun.*, vol. 58, no. 11, pp. 3077–3083, Nov. 2010.

[9] X. Wang and C. Qi, "Algorithm for modeling dual-polarized MIMO channel in land mobile satellite communications," in *Proc. 9th Int. Conf. Wireless Commun. Signal Process. (WCSP)*, Nanjing, China, Oct. 2017, pp. 1–6.

[10] F. P. Fontan, M. Vazquez-Castro, C. E. Cabado, J. P. Garcia, and E. Kubista, "Statistical modeling of the LMS channel," *IEEE Trans. Veh. Technol.*, vol. 50, no. 6, pp. 1549–1567, Nov. 2001.

[11] R. Prieto-Cerdeira, F. Perez-Fontan, P. Burzigotti, A. Bolea-Alamanac, and I. Sanchez-Lago, "Versatile two-state land mobile satellite channel model with first application to DVB-SH analysis," *Int. J. Satell. Commun. Networking*, vol. 28, no. 5-6, pp. 291–315, Sep. 2010.

[12] V. Nikolaidis, N. Moraitis, and A. G. Kanatas, "Statistical characterization of an urban dual-polarized MIMO LMS channel," *Int. J. Satell. Commun. Networking*, vol. 36, no. 6, pp. 474–488, Sep.-Oct. 2018.

[13] M. Sellathurai, P. Guinand, and J. Lodge, "Space-time coding in mobile satellite communications using dual-polarized channels," *IEEE Trans. Veh. Technol.*, vol. 55, no. 1, pp. 188–199, Jan. 2006.

[14] A. Heuberger, "Fade correlation and diversity effects in satellite broadcasting to mobile users in S-band," *Int. J. Satell. Commun. Networking*, vol. 26, no. 5, pp. 359–379, Sep.-Oct. 2008.

[15] M. Vazquez-Castro, F. Perez-Fontan, and S. R. Saunders, "Shadowing correlation assessment and modeling for satellite diversity in urban environments," *Int. J. Satell. Commun. Netw.*, vol. 20, no. 2, pp. 151–166, Mar.-Apr. 2002.

[16] L. Zheng and D. Tse, "Diversity and multiplexing: a fundamental tradeoff in multiple-antenna channels," *IEEE Trans. Inf. Theory*, vol. 49, no. 5, pp. 1073–1096, May 2003.